A new semi-active control based on nonlinear inhomogeneous optimal control for mixed base isolation

Duc Chuan Vu, Ioannis Politopoulos, Sette Diop

Received: 15 September 2016 | Revised: 3 February 2017 | Accepted: 4 April 2017

DOI: 10.1002/stc.2032

RESEARCH ARTICLE

WILEY

A new semi-active control based on nonlinear inhomogeneous optimal control for mixed base isolation

Duc Chuan Vu[1] | Ioannis Politopoulos[1] | Sette Diop[2]

[1] CEA, DEN, DM2S, SEMT, EMSI, Gif-sur-Yvette F-91191, France

[2] CNRS, SUPELEC, Orsay F-91192, France

Correspondence
Ioannis Politopoulos, CEA, DEN, DM2S, SEMT, EMSI, Gif-sur-Yvette F-91191, France.
Email: ipolitopoulos@cea.fr

Funding information
Institut Français de Radioprotection et de Sûreté Nucléaire (IRSN)

Summary

This paper presents a control algorithm for seismic mixed base isolation, combining passive isolators and semi-active viscous dampers. The objective is to limit base displacement while avoiding undesirable amplification of the response of the non-isolated modes. To this end, the proposed algorithm takes into account the constraints on the damping coefficient of the semi-active damper and information on the excitation. It is based on the approximate iterative solution, at each control time step, of a nonlinear inhomogeneous constrained optimal control problem. An autoregressive model is used to obtain, at each control time step, a prediction of the upcoming excitation in a short time interval ahead. Numerical simulation results demonstrate the efficacy of the above method, especially in improving floor response spectra, and its superiority with respect to clipped-optimal algorithms.

KEYWORDS

autoregressive model, floor response spectra, optimal control, seismic isolation, semi-active control

1 | INTRODUCTION

Seismic base isolation is one of the most efficacious seismic mitigation methods. The development and application of this method have grown considerably during the last decades. However, most of the work done on seismic isolation focuses mainly on the impact of the seismic isolation on the main structure itself and much less on the behavior of equipment or components. An outline of previous work on the response of equipment mounted on base isolated structures may be found.[1–4] In the case of industrial and power generation facilities (e.g., nuclear plants), one desirable feature of seismic isolation is to protect sensitive equipment. Actually, floor response spectra corresponding to horizontal excitation will exhibit a local amplification in the vicinity of the isolation frequency, but spectral values for higher frequencies will be on a horizontal plateau. The value of this plateau is approximately the maximum acceleration corresponding to a rigid body mounted on the isolation bearings. This particular shape of floor response spectra is very attractive because it significantly reduces the equipment forces for frequencies higher than about 2 times the isolation frequency and simplifies the analysis and design of equipment. Though the aforementioned ideal floor response spectrum is a good approximation of actual floor spectra for many real seismically isolated structures, in some cases, an amplification of higher modes' response arises that changes this ideal picture and considerably reduces the expected benefit from seismic isolation. The main sources of such an amplification of higher modes response are (a) high base energy dissipation (linear or nonlinear viscous dampers, elastoplastic, or friction dissipative devices),[1–6] as it is often used to reduce base displacement, and (b) rocking induced excitation due to horizontally propagating waves or to the scattered motion in the case of embedded foundation.[7–9] Hence, it would be helpful to find a means to increase base damping avoiding significant amplification of the response of higher modes. As shown in Politopoulos and Pham,[10] a remedy to the above problem could be mixed base isolation, combining passive and active or semi-active devices.[11–14]

In recent years, active structural control strategies have been investigated by numerous researchers because of their performance. However, this is done at the price of high external required power for the actuators to produce the necessary force. An alternative to the full control is the semi-active control (SAC) techniques, which operate with very low supplied power. Much work has been done in the field of semi-active control of structures in general and of base-isolated structures in particular. A family of semi-active control algorithm may be directly obtained by means of Lyapunov's stability theory. The approach requires the use of a Lyapunov function, which must be a positive definite function of the states of the system. The goal of this kind of algorithms is to reduce the responses by minimizing the rate of the Lyapunov function. Several Lyapunov functions may be selected, which may result in a variety of control laws (e.g., bang-bang control,[15] decentralized bang-bang control and its variation—maximum energy dissipation algorithm[16]). Another common way to establish a semi-active control is to extrapolate active control algorithms.[10–14] In a first step, a prediction of the desired control force, $\mathbf{u}^p$, is obtained by an active control algorithm. Then, the characteristics of the semi-active device are adjusted so as to apply a control force, $\mathbf{u}$, that is as close as possible to the predicted force, $\mathbf{u}^p$.

There are many methods available in the literature for designing active controllers. The very popular linear quadratic regulator (LQR)[17,18] determines the control action for a linear system such that a chosen quadratic performance index is minimized. Because the ground acceleration is not known a priori, most applications of LQR have been done using the Riccati closed-loop control, which is, theoretically, valid only when there is no excitation or if the excitation is a white noise random process.[19–21] Of course, earthquake excitations do not meet these conditions. Therefore, in order to improve performance further, the need to take into account the excitation for the controller design arises. However, the earthquake excitation is unknown a priori, yet it may be measured in real time. Possibly, the first attempt to utilize excitation information was made by Yang et al.[22] It is referred to as the instantaneous optimal control algorithms in which a time-dependent performance index is minimized at every time instant. Suhardjo et al.[23] proposed a control algorithm considering a model of the ground acceleration, which consists in filtering a Gaussian white noise process with a Kanai-Tajimi filter. Then, an augmented model composed of the structure's and the excitation's model is considered. This augmented model, excited by a Gaussian white noise disturbance, satisfies the optimality conditions of the Riccati closed-loop control. Then, the optimal control force is obtained as a linear combination of the states of the structure's response and of the excitation model. In particular, the states corresponding to the excitation model may be estimated through an observer where the measured quantity is the ground acceleration. Numerical results based on the above method indicate that its performance is superior to those of Riccati closed-loop control and instantaneous optimal control algorithms. However, in practice, the determination of a reliable excitation model, in advance, is not possible even if geological and seismological data are available. To remedy this inconvenient, Yamada and Kobori[24] and Mei et al.[25] proposed a real-time autoregressive (AR) model of the excitation representing the ground acceleration at each time instant as a linear combination of its previous values. A discrete time controller based on schemes such as the predictive control[26] or the LQR[27] may be applied to the augmented model to determine the control forces. The obtained results confirm that these control algorithms may attenuate the response of structures subjected to seismic excitations.

The main objective of this paper is to propose a semi-active control algorithm for mixed base isolation, combining passive bearings and semi-active dampers, which accounts for the earthquake excitation and avoids amplification of the floor spectral acceleration in the vicinity of the frequencies of the non-isolated modes (i.e., modes other that the modes with small superstructure's deformation at the isolation frequency). At each time step, the ground acceleration is estimated for a short interval ahead by an AR model. Then a damper coefficient is determined by solving the nonlinear inhomogeneous-constrained optimal control problem for this short time interval. Because the control variable is the damper coefficient, the problem is nonlinear (bilinear) even if the passive bearings and the superstructure are considered to be linear. Analytical results give evidence that the proposed method offers advantages over closed loop clipped-optimal control algorithms such as that proposed in another study[10] in improving further the floor response spectra under earthquake excitations.

2 | OPTIMAL CONTROL FOR EARTHQUAKE-EXCITED STRUCTURES

2.1 | Model of the structure

Real base isolated structures are multi-DOF systems. In the case of a stiff superstructure, there are two distinct families of eigenmodes. The first family is that of the isolated eigenmodes at very low frequency, the isolation frequency, with very small deformation in the superstructure. The remaining modes, at higher frequencies, are the non-isolated modes with significant deformation in the superstructure. The simplest model of such a structure, retaining its essential dynamic features, is the two

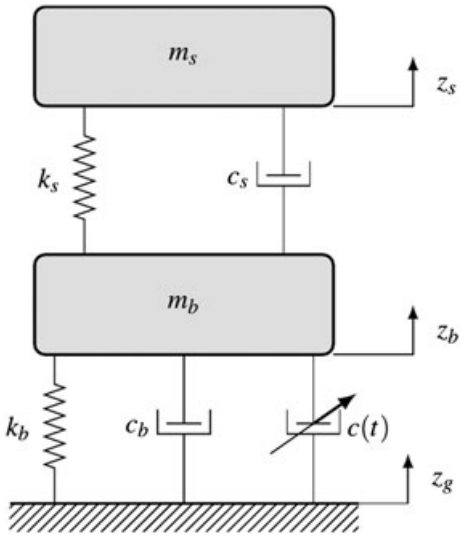

FIGURE 1 Two DOF model of a mixed base isolated structure

DOF model in Figure 1. The upper oscillator represents the first eigenmode of the superstructure if fixed at its base with effective mass m_s, circular frequency $\omega_s = \sqrt{k_s/m_s}$ and critical damping ratio $\xi_s = c_s/\left(2\sqrt{k_s m_s}\right)$. Mass m_b stands for the mass of the second base mat and the residual effective mass corresponding to the higher modes of the superstructure. The spring $k_b = \omega_b^2(m_b + m_s)$ and the damper $c_b = 2\xi_b k_b/\omega_b$ represent the stiffness and damping of isolation devices such as low damping rubber bearings (LDRB). In an effort to reduce the base (mass m_b) displacement without significant amplification of the response of the non-isolated mode, in addition to the LDRB, a linear viscous damper with adaptive damping coefficient $c(t)$ is also considered at the isolation level.

The motion of the structure subjected to one-directional earthquake ground acceleration $w(t) = \ddot{z}_g(t)$, is governed by the following state equation:

$$\dot{x}(t) = Ax(t) + Bu(t) + Ew(t); \qquad x(t_0) = x_0; \qquad x(t) = \begin{bmatrix} v(t) \\ \dot{v}(t) \end{bmatrix}, \tag{1}$$

where $v(t) = [z_b - z_g \ , z_s - z_g]^T$ is the vector of relative displacements with respect to the ground; $x(t)$ is the state vector, and $u(t)$ is the control force generated by the semi-active viscous damper. The matrices A, B, and E read

$$A = \begin{bmatrix} 0_{2\times2} & I_{2\times2} \\ -M^{-1}K & -M^{-1}C \end{bmatrix}; B = \begin{bmatrix} 0_{2\times2} \\ M^{-1}G \end{bmatrix}; E = \begin{bmatrix} 0_{2\times1} \\ M^{-1}H \end{bmatrix}, \tag{2}$$

where M, K, and C are the (2×2) mass, stiffness, and damping matrices, respectively, $G = [1 \quad 0]^T$ is the matrix denoting the location of the semi-active viscous damper and $H = [-1 \quad -1]^T$ is the earthquake excitation input vector, describing the direct influence of the ground acceleration on the structure.

When an idealized semi-active device is assumed (i.e., symmetric response, zero time delay, no force, and displacement limits), the control force is $u(t) = -c(t)\dot{v}_b(t)$ and the state Equation 1 can be rewritten as

$$\dot{x}(t) = [A - c(t)Bb]x(t) + Ew(t), \tag{3}$$

where $c(t)$ is the damping coefficient of the semi-active viscous damper, and $b = [0 \ 0 \ 1 \ 0]$ is the matrix, which denote the location of velocity $\dot{v}_b(t) = \dot{z}_b - \dot{z}_g$ in the state vector.

2.2 | Linear quadratic inhomogeneous active optimal control problem

As already mentioned, the Riccati closed-loop control (solution of LQR), obtained by neglecting the ground acceleration or by considering it as a white noise random process, does not correspond to the optimal control for earthquake-excited structures.

Therefore, in this subsection, we show, following the general procedure described in Bryson and Ho,[18] how the optimal control for the earthquake-excited structure is computed. Of course, in principle, this requires the knowledge of the entire earthquake acceleration history. Let us consider the linear quadratic optimal control problem of the seismically excited system governed by Equation 1:

$$\text{Minimize} \quad J = \int_{t_0}^{t_f} \left(x^T Q x + u^T R u\right) dt + x^T\left(t_f\right) S x\left(t_f\right), \qquad \dot{x}(t) = Ax(t) + Bu(t) + Ew(t); \quad x(t_0) = x_0, \tag{4}$$

where t_f is the final time and S, Q, and R are weighting matrices. S and Q have to be at least positive semidefinite and R positive definite.

The performance index or the so-called cost functional J is a scalar integral function of the state and control variables over the control interval $[t_0, t_f]$. It is minimized with respect to the control force, $u(t)$, while satisfying the constraints specified by the equations of motion of the structure. As shown in other studies,[18,22] the linear quadratic inhomogeneous (LQI) optimal control problem can be analytically solved as follows:

$$u = -R^{-1}B^T[P(t)x + g(t)], \tag{5}$$

where the matrix $P(t)$ and vector $g(t)$ are determined backward from the terminal time t_f by the following expressions:

$$-\dot{P}(t) = P(t)A + A^T P(t) - P(t)BR^{-1}B^T P(t) + Q; \qquad P\left(t_f\right) = S, \tag{6}$$

$$-\dot{g}(t) = \left[A^T - P(t)BR^{-1}B^T\right] g(t) + P(t)Ew; \qquad g\left(t_f\right) = 0. \tag{7}$$

If the control interval $[t_0, t_f]$ is long enough, the time dependent solution $P(t)$ of the differential Riccati Equation 6 may be approximated by the time-independent solution, $\overline{P}$, of the algebraic Riccati equation[20]:

$$0 = \overline{P}A + A^T\overline{P} - \overline{P}BR^{-1}B^T\overline{P} + Q. \tag{8}$$

Of course, for any control interval, if the choice $S = \overline{P}$ is made for the weighting coefficient matrix of the terminal term, there is no transient phase and $P(t) = \overline{P}$.

The Riccati closed-loop control is only a special case of this problem when the excitation, w, in Equation 7 is set to zero. In the general case, Equation 7 should be solved backward from the terminal time t_f and requires the knowledge of the excitation, w, on the entire time interval $[t_0, t_f]$. Consequently, because the earthquake excitation is unknown, the optimal control is not achievable. However, the authors observed that when the control at a sampling instant t_k, $u(t_k)$ is determined by using the actual excitation signal over only a short future time interval of m steps $[t_k, t_{k+m}]$, though the control is no longer, strictly speaking, optimal it, still, maintains a very satisfactory performance as shown in the results presented hereafter. Hence, because the actual signal is not known a priori, the idea of a control based on a real time prediction of the excitation over a short interval ahead arises.

To illustrate the optimal control for the earthquake-excited structure, some numerical examples are presented. The two DOF model in Figure 1 is considered with the following parameters:

$$f_b = 0.5\,Hz, \;\; f_s = 6\,Hz, \quad m_s/(m_b + m_s) = 0.8,$$

where f_b and f_s are the isolation frequency and the frequency of the superstructure, respectively. These frequencies are similar to those commonly met in seismically isolated nuclear plants' buildings. The superstructure's and isolation critical damping ratios are assumed to be equal to 0.05 ($\xi_b = \xi_s = 0.05$). The control objective is to obtain a first mode (isolated mode) response similar to that in the case of additional passive damping while avoiding the undesirable amplification of

the non-isolated modes response. Therefore, the active control force, $u(t)$, is determined by minimizing the cost functional:

$$J = \int_{t_0}^{t_f} \left(\omega_1^2 m_1 q_1^2 + \alpha m_2 \dot{q}_2^2 + Ru^2\right) dt, \tag{9}$$

where $q_{1,2}$ and $m_{1,2}$ are the generalized coordinates and masses of the two modes of the structure, ω_1 is the circular frequency of the first mode, and α and R are penalty coefficients. In order to make a comparison with the LQR solution, the same cost functional as that used in a previous study[10] is considered. To reduce the contribution of the second eigenmode mode to the floor acceleration, a high penalty coefficient α is applied to the kinetic energy of this mode. The penalty coefficient of the control force, R, is tuned so that the first peak of the frequency response of the Riccati close-loop control (peak of the isolated mode) is the same as in the case of a base additional passive damping of 20%. For this study, the chosen values of the penalty parameters are $\alpha = 5 \times 10^5$ and $R = 0.0081$.

Using the transformation between generalized coordinates and relative displacements,

$$q_i = \frac{\varphi_i^T M v}{m_i} \qquad i = 1, 2, \tag{10}$$

where φ_i is eigenvector i, the cost functional can be expressed in terms of the state variables, $x(t) = [v(t) \;\; \dot{v}(t)]^T]$, as follows:

$$J = \int_{t_0}^{t_f} \left(x^T Q x + Ru^2\right) dt, \tag{11}$$

where

$$Q = \begin{bmatrix} (Q_1)_{2\times2} & 0_{2\times2} \\ 0_{2\times2} & (Q_2)_{2\times2} \end{bmatrix}; Q_1 = M^T \left(\frac{\varphi_1 \varphi_1^T \omega_1}{m_1}\right) M; Q_2 = M^T \left(\alpha \times \frac{\varphi_1 \varphi_2^T}{m_2}\right) M. \tag{12}$$

In the rest of the paper, this expression of Q will be considered.

For the first example, we assume that the earthquake excitation is known a priori. One of the Naghan horizontal records of the 1977 Ardal, Iran, earthquake is considered. Its time history and response spectrum normalized with respect to the peak ground acceleration (PGA) are presented in Figure 2. This signal has significant energy in the frequency band where the second eigenfrequency of the structure is located (13.4 Hz). Hence, as confirmed in Figure 3a, a considerable amplification of the response of the second mode will occur if the base passive damping is increased. The control time interval $[t_0, t_f]$ is the whole duration of the considered signal. We compare the performances of LQI and LQR through their respective floor response spectra in Figure 3b,c.

The second example aims at evaluating the control performance when the actual excitation is known only in a short time interval ahead. At each sampling instant t_k, the control force, $u(t_k)$, is determined solving a LQI problem in a time interval $[t_k, t_{k+m}]$. To examine the influence of the duration of the time interval, over which the excitation is known, on the control

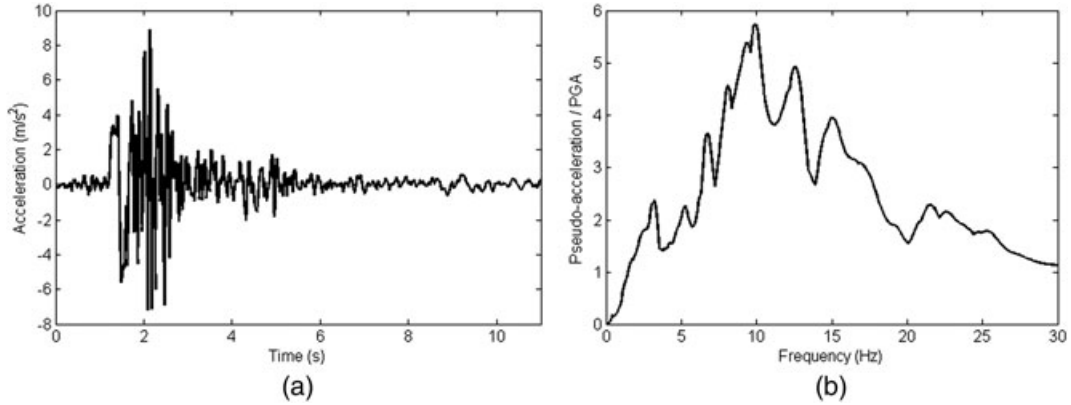

FIGURE 2 Ardal record. (a) Time history and (b) normalized pseudoacceleration response spectrum for 2% damping

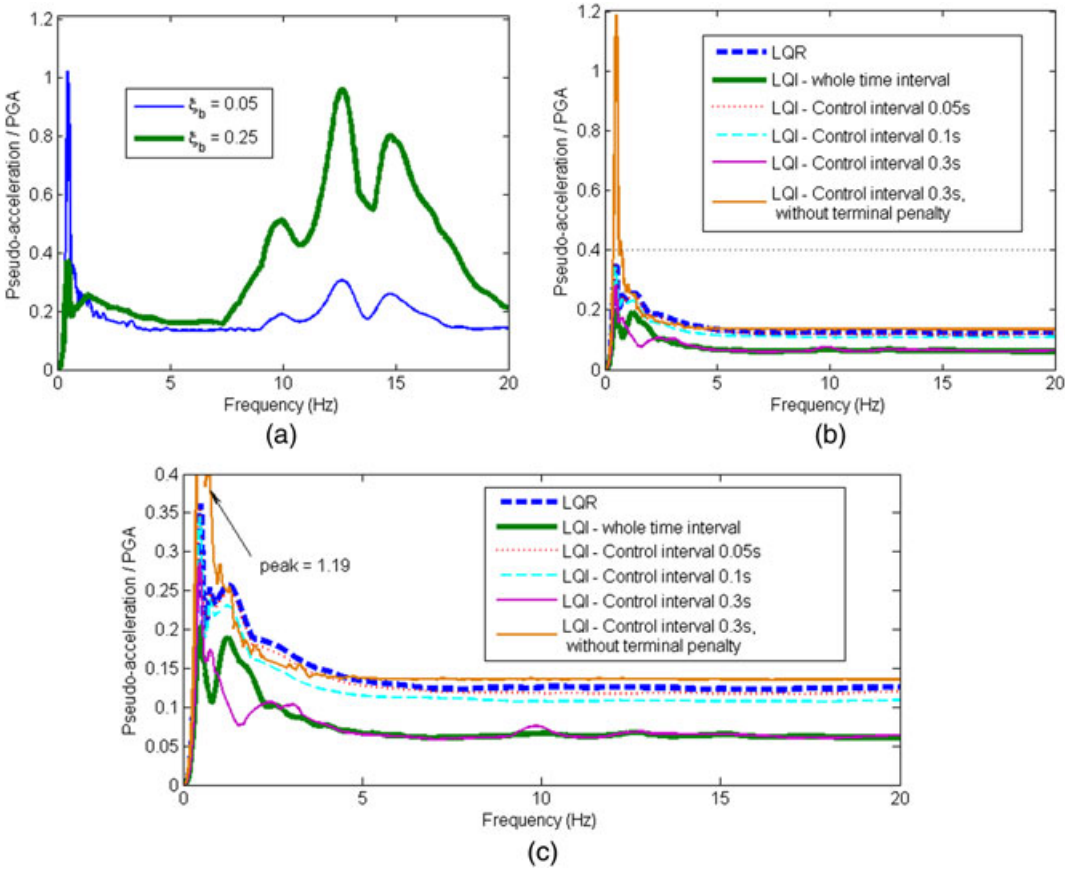

FIGURE 3 Normalized floor response spectrum at the base for the Ardal earthquake for 2% damping. (a) base passive damping; (b) active control; and (c) zoom in on the range of lower pseudoacceleration values of b. LQI = linear quadratic inhomogeneous; LQR = linear quadratic regulator; PGA = peak ground acceleration

efficiency, three different durations, 0.05, 0.1, and 0.3 s, have been considered. To reduce the computational cost, the terminal penalty $x^T\overline{P}x\big|_{t=t_{k+m}}$ has been added to the cost functional. Hence, as already mentioned, the stationary solution $P(t)=\overline{P}$ can be used even if, now, the control interval is short.

In addition, we will show that the use of this final term at each time interval is important to maintain the global control performance when the actual excitation is known only in a short time interval ahead. Actually, the cost functional 11 of the LQI problem reads

$$J=\int_{t_0}^{t_f}\left(x^TQx+Ru^2\right)dt=\int_{t_0}^{t_k}\left(x^TQx+Ru^2\right)dt+\int_{t_k}^{t_{k+m}}\left(x^TQx+Ru^2\right)dt+\int_{t_{k+m}}^{t_f}\left(x^TQx+Ru^2\right)dt. \tag{13}$$

If we assume that up to the current instant t_k the trajectory is optimal, to minimize J one should minimize $J_{t_k}=\int_{t_k}^{t_{k+m}}\left(x^TQx+Ru^2\right)dt+\int_{t_{k+m}}^{t_f}\left(x^TQx+Ru^2\right)dt$. However, the minimization of J_{t_k} is not achievable because the excitation is not known in the whole interval $[t_k,t_f]$ but only in the interval $[t_k,t_{k+m}]$. A local minimization of only the second term in the right hand side (rhs.) of Equation 13 gives poor performance and does not correspond to the minimum of J. Therefore, we approximate the third term on the rhs of Equation 13 with a term depending on the state at t_{k+m}. It turns out that such an approximation is $x^T\overline{P}x\big|_{t=t_{k+m}}$. In fact, because $\overline{P}$ is the solution of the algebraic Riccati Equation 8,

$$\begin{aligned}\frac{d}{dt}\left(x^T\overline{P}x\right)&=\dot{x}^T\overline{P}x+x^T\overline{P}\dot{x}=\left(Ax+Bu+Ew\right)^TPx+x^TP\left(Ax+Bu+Ew\right),\\&=x^T\left(A^T\overline{P}+\overline{P}A\right)x+2x^T\overline{P}Bu+2x^T\overline{P}Ew,\\&=x^T\left(\overline{P}BR^{-1}B^T\overline{P}-Q\right)x+2x^T\overline{P}Bu+2x^T\overline{P}Ew,\end{aligned} \tag{14}$$

and thus

$$\begin{aligned}\int_{t_{k+m}}^{t_f}\left(x^TQx+Ru^2\right)dt &= \int_{t_{k+m}}^{t_f}\left[-\frac{d}{dt}\left(x^T\overline{P}x\right)+\left(x^T\overline{P}BR^{-1}B^T\overline{P}x+2x^T\overline{P}Bu+Ru^2\right)+2x^T\overline{P}Ew\right]dt,\\ &= \left(x^T\overline{P}x\right)\big|_{t=t_{k+m}}-\left(x^T\overline{P}x\right)\big|_{t=t_f}+\int_{t_{k+m}}^{t_f}\left[R\left(u+R^{-1}B^T\overline{P}x\right)^2+2x^T\overline{P}Ew\right]dt,\\ &\approx\left(x^T\overline{P}x\right)\big|_{t=t_{k+m}}.\end{aligned} \tag{15}$$

Consequently, the functional to minimize between t_k and t_f reads

$$J_{t_k}\approx\int_{t_k}^{t_{k+m}}\left(x^TQx+Ru^2\right)dt+\left(x^T\overline{P}x\right)\big|_{t=t_{k+m}}. \tag{16}$$

To examine the influence of the final term on the results, a LQI solution for a time window ahead of 0.3 s, without terminal penalty, which corresponds to the local minimization of only the second term in the rhs of Equation 13, is also considered.

The floor response spectra in Figure 3b,c confirm the beneficial effect of LQI with respect to the enhanced passive damping case shown in Figure 3a. LQI attenuates both the first and second modes' response whose frequencies are 0.5 and 13.4 Hz, respectively. When the excitation is completely known a priori, LQI has a better performance than LQR as shown in Figure 3b,c. It can be noticed that the larger the duration of the excitation known ahead is the better the control performance is (i.e., lower floor spectral values). When the excitation is known over 0.3 s ahead, the achieved performance is almost the same as when entire excitation duration is known. It can be seen in Equation 5 that the effect of the duration of the time interval ahead over which the excitation is known depends on the decay rate of $g(t)$. Hence, it depends, through Equation 7, on the eigenvalues of the matrix $[A^T-P(t)BR^{-1}B^T]$. In other words, it depends on the characteristics of the system and on the weighting matrices in the cost functional. In the same figures, it can be seen that the terminal penalty has an important influence on the control efficiency. In fact, without terminal penalty, LQI for an excitation prediction duration of 0.3 s exhibits a considerably poorer performance.

2.3 | Non-LQI constrained optimal control problem

The aim of this subsection is to present a nonlinear optimal control problem that determines directly the damping coefficient $c(t)$ in Equation 3 and no longer the force u, in the hope of achieving a better control algorithm in the case of bounded values of $c(t)$. In fact, it is the damping coefficient that is the natural control variable of an active damper. Therefore, the general nonlinear Equation 3 will be used. We consider an idealized linear viscous damper (i.e., symmetric response, zero time delay, no force, and displacement limits) with adjustable damping coefficient c, varying from a minimum value c_{min} to a maximum value c_{max}. The following nonlinear quadratic inhomogeneous constrained optimal control problem (NLQI) is considered:

$$\begin{aligned}\text{Minimize}\quad J &= \int_{t_0}^{t_f}x^TQxdt+x\left(t_f\right)^TSx\left(t_f\right),\\ \dot{x} &= f(x,c,t)=[A-c(t)Bb]x(t)+Ew(t);\quad x(t_0)=x_0,\\ c_{\min}&\le c(t)\le c_{\max}.\end{aligned} \tag{17}$$

We see that, in this problem, the Hamiltonian defined as

$$H(x,c,\lambda,t)=x^TQx+\lambda^T[(A-cBb)x+Ew], \tag{18}$$

where λ is the Lagrangian multipliers vector, has a second derivative with respect to the control variable, which is null ($H_{cc}=0$) and that the inequality constraints on the control variable are linear. The optimal control for this problem is of the bang-bang form.[28] Here, we propose a different procedure that, though not strictly optimal, it tends to the optimal solution. In many optimal control algorithms, the Hamiltonian is required to be strictly convex globally with respect to the control variable (i.e., $H_{cc}>0\,\forall\, t\in[t_0,t_f]$; e.g., the successive sweep method of McReynolds and Bryson[29]) or at least to be strictly convex in the neighborhood of its minimum (e.g., Jacobson's algorithm[30]). In order to overcome the convexity restriction, bang-bang control strategies based on differential dynamic programming (DDP) have been proposed in Jacobson.[28] Nevertheless, with our implementation of the algorithm of Jacobson,[28] convergence was achieved only for weighting matrices Q_2 corresponding to small

values of α in Equation 12, whereas, as already mentioned, high values of α are needed to reach the control objective. Therefore, we propose an approximate iterative technique to solve the constrained control problem 17.

Assume that a control variable estimate $\overline{c}(t), \overline{c}\in[c_{\min}, c_{\max}]$ and the corresponding trajectory $\overline{x}(t)$ are available. We define a new regularized optimal control problem:

$$\begin{aligned} \text{Minimize} \quad J_1 &= \int_{t_0}^{t_f} \left[x^T Q x + \varepsilon(c-\overline{c})^2\right] dt + x\left(t_f\right)^T S x\left(t_f\right), \\ \dot{x} &= f(x,c,t) = [A - c(t)Bb]x(t) + Ew(t); \quad x(t_0) = x_0, \\ c_{\min} &\le c(t) \le c_{\max}. \end{aligned} \tag{19}$$

where $\varepsilon > 0$. If the new control problem 19 has a solution $(x_\varepsilon, c_\varepsilon)$, then $J_1(x_\varepsilon, c_\varepsilon) \le J_1(x,c)\,\forall\,(x,c)$. Thus,

$$J_1(x_\varepsilon, c_\varepsilon) \le J_1(\overline{x}, \overline{c}) = \int_{t_0}^{t_f} \overline{x}^T Q \overline{x} dt + \overline{x}\left(t_f\right)^T S \overline{x}\left(t_f\right) = J(\overline{x}, \overline{c}). \tag{20}$$

On the other hand, because $\int_{t_0}^{t_f} \varepsilon(c_\varepsilon - \overline{c})^2 dt \ge 0$, it holds also that

$$J_1(x_\varepsilon, c_\varepsilon) = \int_{t_0}^{t_f} \left[{x_\varepsilon}^T Q x_\varepsilon + \varepsilon(c_\varepsilon - \overline{c})^2\right] dt + x_\varepsilon\left(t_f\right)^T S x_\varepsilon\left(t_f\right) \ge \int_{t_0}^{t_f} {x_\varepsilon}^T Q x_\varepsilon dt + x_\varepsilon\left(t_f\right)^T S x_\varepsilon\left(t_f\right) = J(x_\varepsilon, c_\varepsilon). \tag{21}$$

From relations 20 and 21, it follows that $J(x_\varepsilon, c_\varepsilon) \le J(\overline{x}, \overline{c})$ and thus $c_\varepsilon(t)$ is an improved estimate of $\overline{c}(t)$. Applying this process iteratively leads to estimates of the time history of the control variable corresponding to smaller values of the cost function at each iteration and thus to an approximate solution of the original Equations 17.

The choice of the initial guess of the control variable may be tricky in the general framework of optimal control algorithms. In fact, in a large problem with complicated constraints, the initial guess of the control variable has to be made so that it does not violate any constraint. This is not the case here, because only one simple constraint is considered. Furthermore, because the damping coefficient c varies in a rather narrow range (between c_{min} and c_{max}), it turns out that the procedure is not very sensitive to the initial guess of c. Throughout this work, an initial guess $\overline{c} = (c_{\min} + c_{\max})/2$ has been chosen.

In the following, we briefly present the algorithm used to solve the regularized optimal control problem 19. For the sake of generality, we consider the following problem:

$$\begin{aligned} \text{Minimize} \quad J_1 &= \int_{t_0}^{t_f} L(x,c,t) dt + \psi\left[x\left(t_f\right), t_f\right], \\ \dot{x} &= f(x,c,t); \quad x(t_0) = x_0, \\ c_{\min} &\le c(t) \le c_{\max}, \end{aligned} \tag{22}$$

where $L(x,c,t)$ is a function of x, c, and t, and $\psi[x(t_f), t_f]$ depend only on the final time t_f.

First, the unconstrained optimal control problem is considered. Because of the nonlinearity, the unconstrained control problem cannot be solved analytically (i.e., it is not possible to obtain a closed form solution as it was the case for Equation 5). Therefore, we focus on its numerical solution. It has been shown that the necessary optimality conditions for the optimal control problem without constraints lead to a two-point boundary value problem.[17,18] This two-point boundary value problem can be directly solved by several numerical schemes, but the amount of computation may be too high if the number of variables is big or if the control interval is long. Actually, for real time control, the computational time at each time step must be very low. An efficient way to overcome this inconvenient is offered by iterative algorithms in which estimates of the control histories are improved iteratively so as to come closer to satisfying the necessary optimality conditions. McReynolds and Bryson[29] proposed the successive sweep method that gives improved estimates of the control variable so that the gradient of the Hamiltonian becomes smaller at each step. Thus, after a finite number of steps, the gradient of the Hamiltonian can be made very small, practically zero, as required for optimality.

The solution of optimal control problems becomes, in general, more difficult in the presence of side constraints. Such constraints are commonly met in practice because of physical limitations of the control devices. A drawback with the McReynolds and Bryson's method is that it cannot handle directly inequality constraints on control variables. Instead, inequality constraints have to be approximated by penalty functions.[30] To overcome this drawback, Jacobson[30] developed a method using the notion of DDP. For the sake of completeness, in the following, the basic steps of the method are presented.

In DDP, we define a scalar function V of time t ($t \in [t_0, t_f]$) and of the state vector $x(t)$ to be the cost functional considering that the initial state is $x(t)$

$$V(x,t) = \int_t^{t_f} L[x(\tau), c(\tau), \tau] d\tau + \psi\left[x\left(t_f\right), t_f\right], \tag{23}$$

and thus

$$J_1 = \int_{t_0}^{t_f} L(x,c,t)dt + \psi\left[x\left(t_f\right), t_f\right] = V(x_0, t_0). \tag{24}$$

Assume that x^o is the optimal state trajectory corresponding to the optimal control c^o. It is well known[17,18] that the optimal cost $V^o(x_0, t_0)$ satisfies the following Hamilton–Jacobi–Bellman partial differential equation:

$$-\frac{\partial V^o}{\partial t}(x^o, t) = \min_{c \in [c_{\min}, c_{\max}]} \left[L(x^o, c, t) + V_x^o(x^o, t)^T f(x^o, c, t)\right], \tag{25}$$

where V_x is the derivate with respect to x of function $V(x,t)$. The Hamiltonian is defined as

$$H(x, c, V_x, t) = L(x, c, t) + {V_x}^T f(x, c, t). \tag{26}$$

Assuming that the optimal control $c^o(t)$ exists, is unique and continuous in the interval $[t_0, t_f]$, the solution of the optimal control problem with inequality constraints on the control variables (Equations 22) is obtained by Jacobson's method[30] as follows:

Step 1a. Guess a control history $\widetilde{c}(t), \widetilde{c} \in [c_{\min}, c_{\max}]$ $\forall t$ and integrate the system equations $\dot{x} = f(x,c,t)$ with the specified initial condition $x(t_0) = x_0$ to obtain the corresponding trajectory $\widetilde{x}(t)$ and performance index $\widetilde{J}_1$.

Step 1b. Using the initial conditions

$$V_x\left(t_f\right) = \psi_x\left[\widetilde{x}\left(t_f\right), t_f\right] \text{ and } V_{xx}\left(t_f\right) = \psi_{xx}\left[\widetilde{x}\left(t_f\right), t_f\right], \tag{27}$$

integrate backwards from t_f to t_0 the following equations:

$$\begin{cases} -\dot{V}_x = H_x(\widetilde{x}, \widehat{c}, V_x, t) + V_{xx}[f(\widetilde{x}, \widehat{c}, t) - f(\widetilde{x}, \widetilde{c}, t)], \\ -\dot{V}_{xx} = H_{xx}(\widetilde{x}, \widehat{c}, V_x, t) + [f_x(\widetilde{x}, \widehat{c}, t)]^T V_{xx} + V_{xx} f_x(\widetilde{x}, \widehat{c}, t), \end{cases} \tag{28}$$

while minimizing $H(\widetilde{x}, c, V_x, t)$ with respect to c, subject to $c \in [c_{\min}, c_{\max}]$ to obtain $V_x(t)$ $V_{xx}(t)$, and an improved estimate of the control variable $\widehat{c}(t)$. The differential Equation 28 is established by introducing the second-order expansions of $V(x,t)$ about $(\widetilde{x}, \widehat{c})$ into the Hamilton–Jacobi–Bellman equation.[29] To solve, Equation 28 recall that $\widetilde{x}(t)$ has been computed in Step 1a. Then, going back from the final time t_f, at each sampling instant t_{k+1} the explicit forward Euler's scheme may be used to compute $V_x(t_k)$ and $V_{xx}(t_k)$. Eventually, $\widehat{c}(t_k)$ is obtained by the constrained minimization of $H[\widetilde{x}(t_k), c, V_x(t_k), t_k]$ which is a nonlinear function of c. This constrained minimization is a nonlinear programming problem. For complicated forms of Hamiltonian, with several constraints, the reader can refer to methods of feasible directions.[31] In the present case (Equations 19), the corresponding Hamiltonian $H(\widetilde{x}, c, V_x, t)$ is of second order in c. Therefore, its minimum with respect to c is the minimum of a quadratic function in the interval $[c_{\min}, c_{\max}]$. It occurs at one of the two extremities of the segment corresponding to $c_{\min}$ or $c_{\max}$ unless the vertex of the parabola lies between these two values.

Step 1c. Using $\widehat{c}(t)$, calculate the corresponding trajectory $\widehat{x}(t)$, the performance index $\widehat{J}_1$, and the improvement index $\tau = \dfrac{\widetilde{J}_1 - \widehat{J}_1}{\widetilde{J}_1}$.

Step 1d. Replace the old $\widetilde{c}(t), \widetilde{x}(t), \widetilde{J}_1$ with $\widehat{c}(t), \widehat{x}(t), \widehat{J}_1$ and repeat Steps 1b–d until τ reaches the desired accuracy.

According to Jacobson,[30] if the differential Equations 28 has bounded solutions, the sufficient conditions to reduce the cost functional with this procedure are

1. $H(\widetilde{x}, \widehat{c}, V_x, t) < H(\widetilde{x}, \widetilde{c}, V_x, t)$, $\widehat{c} \neq \widetilde{c}$. This condition is met because $\widehat{c}$ results from the minimization of $H(\widetilde{x}, c, V_x, t)$.
2. $H_{cc}(\widetilde{x}, \widehat{c}, V_x, t)$ is positive definite. This condition is always satisfied for the problem 19 because $H_{cc}(x, c, V_x, t) = 2\varepsilon > 0$.

In the practical implementation of the method, we do not solve entirely problem 19 but we stop at Step 1c. That is, we limit ourselves to the first only estimate of $\widehat{c}(t)$ and $\widehat{J}_1$ which gives $\tau > 0$. It is reminded that our goal is not to solve exactly problem 19 but to solve the original problem 17 taking benefit from relations 20 and 21. Actually, these relations hold, not only for the solution $(x_\varepsilon, c_\varepsilon)$ of Equation 19 but also for any set (x, c) such that, with the notations in Equations 19–21, $J_1(x,c) \leq J_1(\overline{x}, \overline{c})$ (i.e. $\tau > 0$). However, it is not always possible to achieve $\tau > 0$ for any value of ε. In fact, because, in the cost function, ε is the weighting coefficient of the variation of the control variable with respect to its reference $\overline{c}(t)$, small values of ε authorize important changes of c and thus of the state variables x. But, as already mentioned, Equation 28 is valid for small variations of x with respect to $\widetilde{x}$. Hence, if $\tau < 0$, ε is increased until $\tau > 0$.

As already shown, applying the above procedure successively leads to successive improved estimates of the control variable of the initial NLQI problem 17. The method to solve problem 17 is outlined below:

Step 2a. Guess a control history $\overline{c}(t), \overline{c} \in [c_{\min}, c_{\max}]\ \forall t$ and integrate the system equations $\dot{x} = f(x, \overline{c}, t)$ with the specified initial condition $x(t_0) = x_0$ to obtain the corresponding trajectory $\overline{x}(t)$ and performance index $\overline{J}$.

Step 2b. Choose an initial value of ε.

An estimate of the initial value of ε may be obtained so that the second term $\varepsilon(c-\overline{c})^2$ in the cost functional of problem 19 is much (e.g., one order of magnitude or more) smaller than the first one, $x^T Q x$. The latter is always higher than the potential energy of the isolators, $x^T Q x > \omega_b^2 (m_s + m_b) x_b^2$, and the order of magnitude of the base displacement x_b may be given by the static response approximation $\ddot{x}_g/\omega_b^2$. On the other hand, $\varepsilon(c-\overline{c})^2 \leq \varepsilon(c_{\max}-c_{\min})^2$. Hence, a good choice is $\varepsilon << \ddot{x}_g^2/[\omega_b(c_{\max}-c_{\min})]^2$. Throughout this work, we considered as initial value $\varepsilon_0 = 0.01\left\langle \ddot{x}_g^2 \right\rangle/[\omega_b(c_{\max}-c_{\min})]^2$, where $\left\langle \ddot{x}_g^2 \right\rangle$ is the mean square of the excitation or its prediction (Section 3) in the control interval.

Step 2c. Using the guessed control history $\overline{c}(t)$, apply Step 1a–c to obtain $c_\varepsilon(t), x_\varepsilon(t), J(x_\varepsilon, c_\varepsilon)$. As discussed above, if in Step 1c $\tau < 0$, ε is increased until $\tau > 0$. Compute the degree of improvement, $\kappa = \dfrac{\overline{J} - J(x_\varepsilon, c_\varepsilon)}{\overline{J}}$.

Step 2d. Replace the old $\overline{c}(t), \overline{x}(t), J(\overline{x}, \overline{c})$ with $c_\varepsilon(t), x_\varepsilon(t), J(x_\varepsilon, c_\varepsilon)$ and repeat Step 2c,d using the value of ε of the last iteration until κ becomes smaller than a convergence tolerance value (e.g., $\kappa < 10^{-5}$). However, small values of κ may indicate either convergence or, on the contrary, poor convergence rate. If, at the same time, ε is smaller than a given threshold (e.g., $\varepsilon < \varepsilon_0$), convergence is assumed and the solution is $c = c_\varepsilon$. Otherwise, successive trials with smaller values of ε are made in Step 2c until $\varepsilon < \varepsilon_0$ or as far as $\tau > 0$ in Step 1c. If, after these trials, κ remains lower than the convergence tolerance, convergence is assumed. Otherwise, the iterative process goes on.

Similar to the linear inhomogeneous optimal problem discussed in the previous subsection, the solution of the nonlinear inhomogeneous optimal control problem requires the excitation $w(t)$ over the entire control interval $[t_0, t_f]$ to be known a priori. To illustrate the application of the above algorithm, we consider again the two DOF model in Figure 1 with the same structural properties and excitation as in subsection 2.2.

The damping coefficient of the semi-active damper, $c(t)$, will be determined by solving, using the above approximate method, the following problem:

$$\begin{aligned} \text{Minimize } J &= \int_{t_0}^{t_f} x^T Q x dt. \\ \dot{x} &= f(x, c, t) = [A - c(t) B b] x(t) + E w(t); \quad x(t_0) = x_0, \\ & c_{\min} \leq c(t) \leq c_{\max}. \end{aligned} \tag{29}$$

A first numerical example is studied assuming that the earthquake excitation is known a priori. The same weighting matrix Q, described in Equation 12 in subsection 2.2, with a penalty coefficient $\alpha = 5 \times 10^5$, is chosen. We consider a viscous damper with an adjustable coefficient, $c(t)$, corresponding to an additional base critical damping ratio, $\xi_b^{add} = c\omega_b/2k_b$, varying in the range 0–0.20. Therefore, $c_{\min} = 0$ and $c_{\max} = 0.20 \times 2k_b/\omega_b$. The control time interval $[t_0, t_f]$ is the duration of the considered signal.

A second example investigates the control performance when the actual excitation is known only over a short time interval ahead. At each sampling instant, t_k, the damping coefficient, $c(t_k)$, is determined solving the nonlinear inhomogeneous optimal control problem 29 in the time interval $[t_k, t_{k+m}]$. To examine the influence of the duration of the time interval on the control efficiency, three different durations, 0.05, 0.1, and 0.3 s, have been considered. As in subsection 2.2, the final term $x^T \overline{P} x\big|_{t=t_{k+m}}$ where $\overline{P}$ is the solution of the algebraic Riccati Equation 8 is added to the cost functional of each time interval $[t_k, t_{k+m}]$. In fact,

with the same reasoning (Equations 14–16), it can be shown that this final term at each time interval is important to maintain the global control performance for the NLQI problem 28 when the actual excitation is known only in a short time interval ahead.

The floor response spectra in Figure 4a show that, when the excitation is known a priori, the nonlinear control of the damping coefficient of the semi-active damper (NLQI) has a performance comparable to that of LQR in the vicinity of the second eigen frequency (13.4 Hz). However, it results in a higher peak at the isolation frequency (0.5 Hz). As already mentioned in subsection 2.2 and also shown in Figure 4a, LQI has a better performance than LQR. It is also observed that, when the entire excitation is known, the efficacy of NLQI is inferior to that of LQI. This was expected because NLQI is a semi-active control with restrictions on the damping coefficient, which are not taken into account in LQI. The floor response spectra in Figure 4b show that the performance of NLQI is not degraded significantly when the excitation is known over only a short time interval ahead (except in the case of a very short interval, 0.05 s). It is worth noting that although LQI needs to know the excitation ahead at least for 0.3 s to achieve a satisfactory performance (Figure 3b subsection 2.2), NLQI gives satisfactory results even for a much smaller duration of 0.1 s. Therefore, this duration of the control time window will be considered in the remaining part of the paper. In the same Figure 4b, it can be seen that, as it was the case for LQI (Figure 3). without terminal penalty, NLQI exhibits also a considerably poorer performance.

The floor response spectra presented in Figure 4 have been normalized with respect to the PGA. In fact, it can be shown that, despite the nonlinearity, the control variable solution of the NLQI problem 29, $c(t)$, does not depend on the PGA. Let us consider the NLQI problem 29 whose solution is the damping coefficient $c(t)$ and the system's state $x(t)$ corresponding to the minimum of the cost function $J_{\min}$. If the excitation is multiplied by a factor μ (i.e., $\widetilde{w} = \mu w$), the solution of the NLQI problem will give a new optimum solution $\widetilde{c}(t)$, $\widetilde{x}(t)$, and $\widetilde{J}_{\min}$. On the other hand, multiplying Equation 29 by μ shows that if the control $c(t)$ is applied under the excitation $\widetilde{w} = \mu w$, the corresponding state trajectory and cost functions will be $\mu x(t)$ and $\mu^2 J_{\min}$. Because the cost function corresponding to the optimal solution under excitation $\widetilde{w}$ is $\widetilde{J}_{\min}$, it follows that $\mu^2 J_{\min} \geq \widetilde{J}_{\min}$. With the same reasoning, if the control $\widetilde{c}(t)$ is applied under excitation $w = \widetilde{w}/\mu$, the corresponding state trajectory and cost functions will be $\widetilde{x}(t)/\mu$ and $\widetilde{J}_{\min}/\mu^2 \geq J_{\min}$. The only possibility to meet both the above inequalities is $\widetilde{J}_{\min} = \mu^2 J_{\min}$ and thus $\widetilde{x}(t) = \mu x(t)$ and $\widetilde{c}(t) = c(t)$. Consequently, the optimal damping coefficient is independent of the excitation multiplier μ.

Last, a third example investigates the influence of the initial conditions. Actually, in most real structural control implementations, in general, a decision has to be made regarding the start moment of the control procedure. Typically, the control procedure may start when one or more measures (e.g., base displacement and/or acceleration and/or ground acceleration in the present case) reach a threshold. Then, for the proposed method, the initial conditions for the equation of motion 3 will be the state vector at that moment. As shown in Figure 5, simulations with two different initial conditions, corresponding to the time instants where the excitation acceleration is 0 and 0.02 g, respectively, result in quasi-identical control and system's state history.

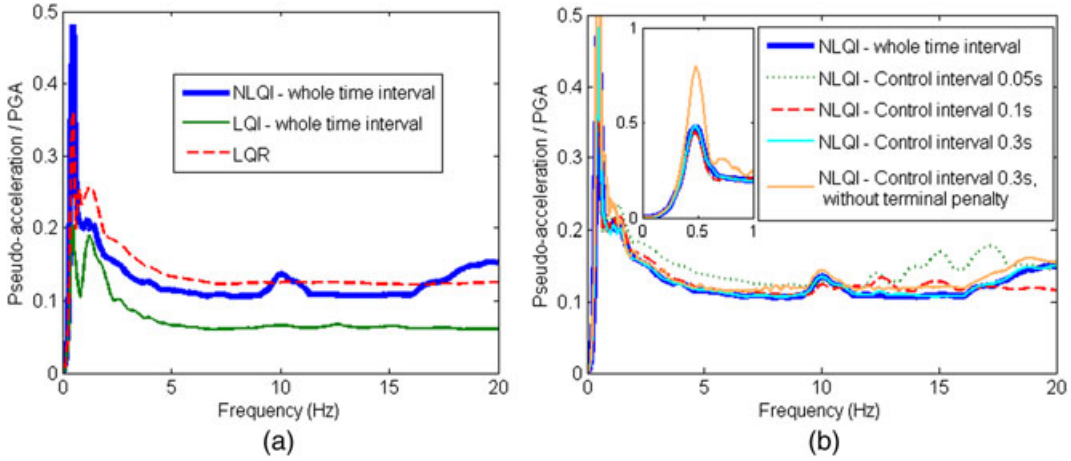

FIGURE 4 Normalized floor response spectrum at the base for the Ardal earthquake for 2% damping. (a) Comparison between linear and nonlinear optimal control when the excitation is known over the whole control time duration and (b) nonlinear optimal control when the excitation is known over a short time interval. LQI = linear quadratic inhomogeneous; LQR = linear quadratic regulator; NLQI = nonlinear quadratic inhomogeneous; PGA = peak ground acceleration

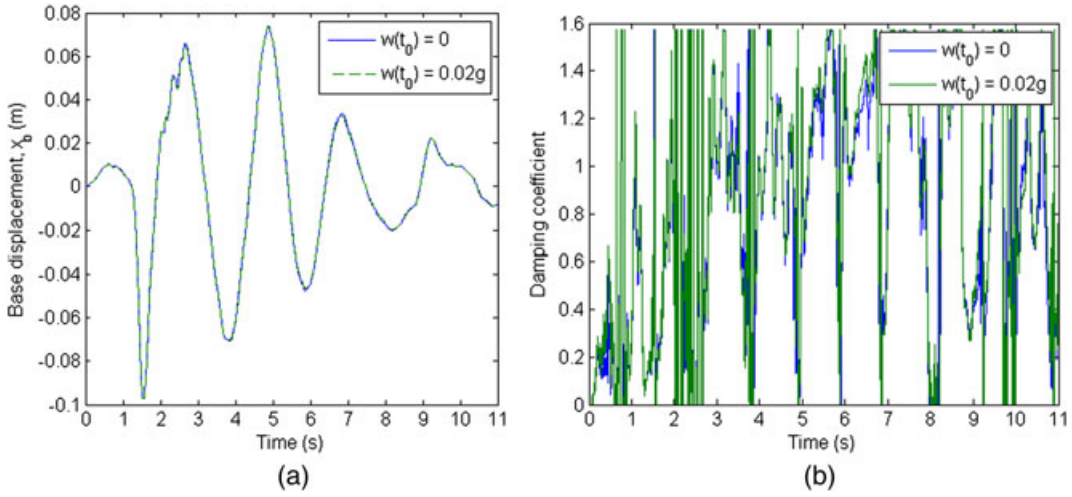

FIGURE 5 Influence of the initial conditions (a) base displacement and (b) damping coefficient of the semi-active device

2.4 | Nonlinear versus clipped linear semi-active controls

As already mentioned, the results presented in Figure 4a show that the efficacy of the linear optimal inhomogeneous control is superior to that of the nonlinear optimal inhomogeneous control at least when the whole excitation signal is assumed to be known. However, it is reminded that our goal is semi-active and not active control. To this end, we are interested in clipped-like algorithms that determine the damping coefficient of a SAC damper based on the solution of the above LQI active control problem. We consider the two DOF model in Figure 1 with the same properties and excitation as in subsection 2.2 and a viscous damper with the same properties as in subsection 2.3. At each sampling instant t_k, a desired active control force, $u^p(t_k)$, is determine solving LQI in the 0.1 s time interval ahead $[t_k, t_k + 0.1\,s]$ as it is done in the second example of subsection 2.2. The excitation in this control time interval is supposed to be known. The semi-active damping coefficient is then adjusted so as to apply a control force, $u(t_k) = -c(t_k)\dot{v}_b(t_k)$, that is as close as possible to the predicted force, $u^p(t_k)$:

$$\begin{aligned}&\text{if } u^p\dot{v}_b<0 \text{ and } |u^p|<c_{\max}|\dot{v}_b|,\ c(t_k) = |u^p|/|\dot{v}_b|,\\ &\text{if } u^p\dot{v}_b<0 \text{ and } |u^p|\geq c_{\max}|\dot{v}_b|,\ c(t_k)=c_{\max},\\ &\text{if } u^p\dot{v}_b\geq 0,\ c(t_k)=c_{\min},\end{aligned}$$

where $c_{\min}$ and $c_{\max}$ are, respectively, the minimum and maximum damping coefficients. In the following, this control will be noted SAC LQI. We consider also the clipped-optimal control,[11–13] which is realized as above except that the desired control force, $u^p(t_k)$, is calculated by LQR. This control will be noted SAC LQR.

The results of these clipped controls are compared to those obtained by the nonlinear control algorithm described in the previous section. The damping coefficient of the semi-active damper, $c(t_k)$, is directly obtained at each instant t_k by solving the NLQI problem in the time interval $[t_k, t_k + 0.1\,s]$ as it is done in the second example of the subsection 2.3. Once again, the upcoming excitation in this control time interval is supposed to be known.

The results in Figure 6 show that SAC LQI control exhibits a trend that is the opposite of that observed for LQI. As already shown in Figure 4a, when the entire excitation is known, the efficacy of NLQI is inferior to that of LQI, as far as the attenuation of both first and second modes' response is concerned. On the other hand, NLQI has a superior performance to that of SAC LQI when the excitation is supposed to be known only over a short time interval (0.1 s) ahead the current time step. Actually, in comparison with SAC LQI, NLQI results in the same peak amplitude at the first eigen frequency (0.5 Hz) whereas it performs considerably better at frequencies higher that 8 Hz. This confirms that the nonlinear optimal control, which permits to determine directly the damping coefficient while accounting for device's constraints, is more relevant than clipped controls. In the same figure, it can be seen that, compared to SAC LQR, SAC LQI has also a slight beneficial effect on the attenuation of the response at frequencies higher that 10 Hz.

All above calculations have a theoretical interest because they allow us to gain a further insight into the efficacy of the discussed control techniques. However, regarding the inhomogeneous control techniques, in practice, seismic excitation is not known a priori. Therefore, the need for estimating, in real time, the upcoming excitation, at least over a short time interval arises. Such a prediction model, to be used in conjunction with the above control techniques, is discussed in the next section.

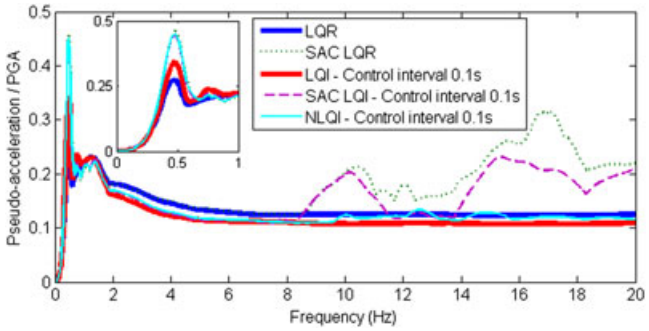

FIGURE 6 Normalized floor response spectrum at the base for the Ardal earthquake for 2% damping. LQI = linear quadratic inhomogeneous; LQR = linear quadratic regulator; NLQI = nonlinear quadratic inhomogeneous; PGA = peak ground acceleration; SAC = semi-active control

3 | AR EXCITATION MODEL

3.1 | AR prediction

The success with which a signal can be predicted from its past samples depends on the power spectrum of the signal. In general, the more correlated or predictable a signal, the more concentrated its power spectrum, and conversely, the more random or unpredictable a signal, the more spread its power spectrum.[32] Of course, seismic excitations present random characteristics, and they are not narrow band processes. Nevertheless, in general, their spectrum presents an amplification within a limited frequency band. Therefore, it may be hoped that they could be predicted to some extent. The aim of this section is to present and discuss the prediction model and the calculation of the predictor coefficients applied in this work. To this end, we follow the general theory of AR models presented in Vaseghi.[32]

At a sampling time $t_k = k\Delta t$, the excitation signal value $w_k = w(t_k)$ can be written as a linear combination of past p samples and a residual or error term, e_k:

$$w_k = a_1 w_{k-1} + a_2 w_{k-2} + \cdots + a_p w_{k-p} + e_k = \sum_{i=1}^{p} a_i w_{k-i} + e_k. \tag{30}$$

Equation 30 represents an AR model of order p. A prediction of w_k consistent with the above AR model is given by

$$\widehat{w}_k = \sum_{i=1}^{p} a_i w_{k-i}, \tag{31}$$

where $\{a_1, a_2, \ldots, a_p\}$ are the prediction coefficients of the AR model. Then, the prediction error reads

$$e_k = w_k - \widehat{w}_k = w_k - \sum_{i=1}^{p} a_i w_{k-i}. \tag{32}$$

The prediction given by Equation 31 is also called forward prediction. Similarly, we can define a backward predictor that predicts a sample $w_{k-p} = w(t_{k-p})$ from p future samples $w_{k-p+1}, \ldots, w_k$:

$$\widehat{w}_{k-p} = \sum_{i=1}^{p} c_i w_{k-i+1}. \tag{33}$$

The corresponding backward prediction error reads

$$b_k = w_{k-p} - \widehat{w}_{k-p} = w_{k-p} - \sum_{i=1}^{p} c_i w_{k-i+1}. \tag{34}$$

The coefficients of the AR model can be derived through least square techniques from a signal block of N samples $\{w_{k-1}, w_{k-2}, \ldots, w_{k-N}\}$ (e.g., Yule–Walker method[33] and Burg's method[32]). Burg's method, which is used in this work, is a recursive order-update method that computes the coefficients of a predictor of order i, using the coefficients

of a predictor of order $i-1$. This is done by minimizing the sum of the squared forward and backward prediction errors of a predictor of order i defined as

$$E^{(i)} = \sum_{n=k-N}^{k-1} \left\{ [e_{n^{(i)}}]^2 + [b_{n^{(i)}}]^2 \right\}, \quad 0 \le i \le p. \tag{35}$$

The outcome of this minimization, which permits to compute the predictor coefficients $\{a_1, a_2, \ldots, a_p\}$, reads

$$\begin{aligned} & e_{n^{(0)}} = b_{n^{(0)}} = w_n \;\; ; \;\; e_{n^{(i)}} = e_{n^{(i-1)}} - h_i b_{n-1^{(i-1)}} \;\; ; \;\; b_{n^{(i)}} = b_{n-1^{(i-1)}} - h_i e_{n^{(i-1)}} \quad (k-N \le n \le k-1), \\ & h_i = 2 \sum_{n=k-N}^{k-1} e_{n^{(i-1)}} b_{n-1^{(i-1)}} \Big/ \sum_{n=k-N}^{k-1} \left\{ [e_{n^{(i-1)}}]^2 + [b_{n-1^{(i-1)}}]^2 \right\}, \\ & a_{i^{(i)}} = h_i \;\; ; \;\; a_{j^{(i)}} = a_{j^{(i-1)}} - h_i a_{i-j^{(i-1)}} \qquad (1 \le j \le i-1), \\ & a_j = a_{j^{(p)}} \qquad (1 \le j \le p). \end{aligned} \tag{36}$$

In order to obtain a prediction of the seismic excitation in the interval $[t_k, t_{k+m}]$, having measured values only up to t_{k-1}, we coincide $w_k = \widehat{w}_k$, estimate $\widehat{w}_{k+1}$ by Equation 31 with the same prediction coefficients, and repeat the procedure until t_{k+m} as illustrated in Figure 7.

3.2 | Parametric study of the AR model

When a signal block of past N samples $\{w_{k-N}, \ldots, w_{k-2}, w_{k-1}\}$ is available, one procedure to determine the adequate model order p is to increment the model order and monitor the increment of the squared error $E^{(i)}$, until it levels off.[32] The increment of the squared error with increasing model order from $i-1$ to i reads

$$\Delta E^{(i)} = E^{(i-1)} - E^{(i)}. \tag{37}$$

The order p beyond which $\Delta E^{(p)}/E^{(0)}$ becomes less than a threshold is taken as the adequate model order. Herein, this procedure is applied for each control time interval and thus the order of the AR model varies with time. Figure 8a illustrates the decrease of $\Delta E^{(i)}/E^{(0)}$ with increasing model order for the prediction in the interval [5.0 s, 5.1 s] of the Ardal record, using a

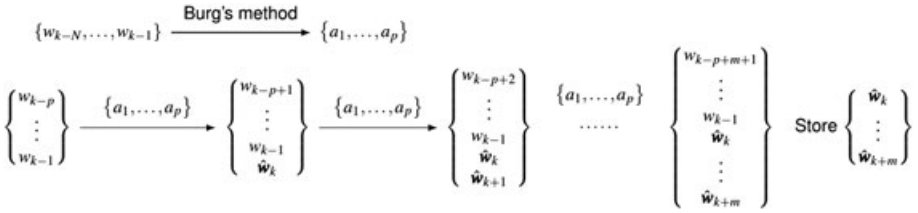

FIGURE 7 Prediction procedure of the seismic excitation signal for the interval $[t_k, t_{k+m}]$

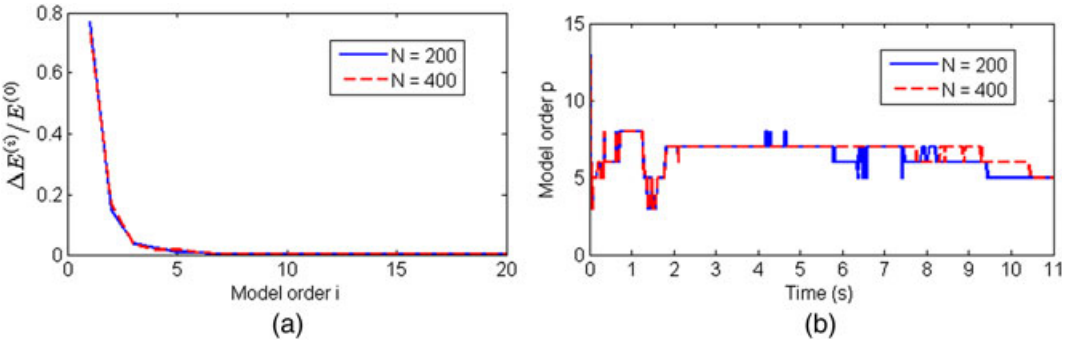

FIGURE 8 AR model order for the Ardal record a) decrease of the normalized squared prediction error with increasing model order for the interval [5.0 *s*, 5.1 *s*]. b) determined model order vs time

block of past 200 and 400 samples (sampling period $\Delta t = 0.01$ s). Figure 8b shows the AR model order determined by this procedure at each time instant for the same prediction window duration of 0.1 s.

To examine what could be a reasonable (satisfactory computational cost-accuracy trade off) number N of past samples to take into account for the determination of the coefficients of the AR model, we carried out some tests considering several values of N. To this end, because the control at instant t_k depends on the predicted excitation in the interval $[t_k, t_{k+m}]$, a local prediction error index could be defined as the root mean square of the prediction errors for all samples, $t_k, t_{k+1}, \ldots, t_{k+m}$, in this interval:

$$\eta(t_k) = \sqrt{\frac{1}{m+1}\left[(w_k - \widehat{w}_k)^2 + (w_{k+1} - \widehat{w}_{k+1})^2 + \cdots + (w_{k+m} - \widehat{w}_{k+m})^2\right]}. \tag{38}$$

The above Ardal record, two of the horizontal acceleration signals recorded during the main event of the Tohoku, Japan, earthquake on 11/03/2011 and two artificially generated signals compatible with a rock site in south France (Cadarache) are considered. The sample period is $\Delta t = 0.01\,s$. For each signal, we consider several values of N; we calculate the corresponding local prediction error index $\eta(t)$ for each time instant and then its root mean square σ over time normalized with respect to the PGA. The mean of the normalized prediction errors of the above five signals, $\overline{\sigma}$, is plotted in Figure 9.

As expected, the prediction is, in general, better when we use more past excitation information. However, increasing N beyond a certain number, around 250 in the present case, does not result in a significant improvement. Consequently, to limit the computational cost, it may be concluded that $N = 250$ is an appropriate value for practical use. Figure 10 shows the predicted signal, in the case of the Ardal record, for the time intervals [3.0 s, 3.1 s] and [6.0 s, 6.1 s]. It may be observed that the predicted signal presents non-negligible differences with respect to the actual signal. However, as discussed in the following section, despite this divergence, the final outcome of interest that is the response of the semi-actively controlled structure is quite satisfactory.

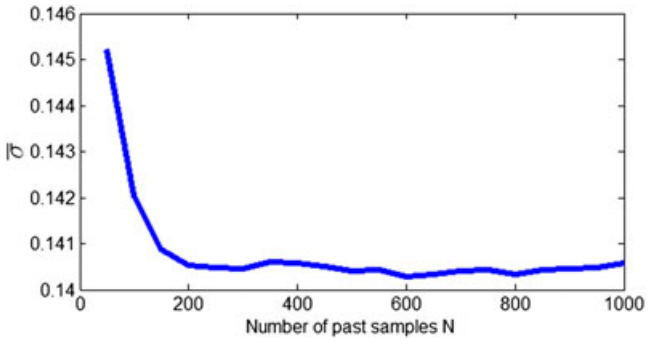

FIGURE 9 Mean normalized prediction error for the considered five signals

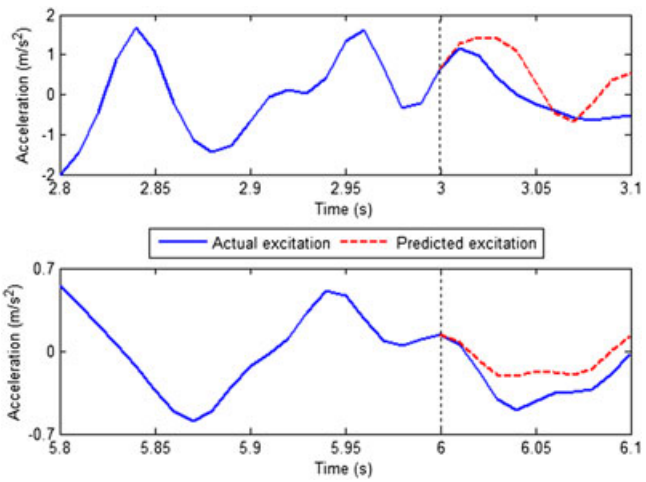

FIGURE 10 Comparison between predicted and actual excitation for Ardal earthquake

4 | FLOOR RESPONSE SPECTRA

Once a prediction of the excitation in the interval $[t_k, t_{k+m}]$ is determined, the semi-active control algorithm presented in subsections 2.3 and 2.4, based on the solution of the NLQI problem, may be applied. At instant $t_k = k\Delta t$, the damping coefficient is computed as follows:

Step 1. Solve the identification problem of the AR model for the excitation window $\{w_i: i = k-N \text{ to } k-1\}$, to obtain the model order p, the predictor coefficients $\{a_i: i = 1 \text{ to } p\}$ and estimate the excitation in the interval $[t_k, t_{k+m}]$ $\{\widehat{w}_i: i = k \text{ to } k+m\}$.

Step 2. Using the estimated excitation $\{\widehat{w}_i: i = k \text{ to } k+m\}$, solve NLQI in the control interval $[t_k, t_{k+m}]$ and get the damping coefficient $c(t_k)$.

Numerical simulations are carried out to demonstrate the efficacy of the proposed semi-active control algorithm with respect to the floor response spectra of base isolated structures. We consider again the two DOF model of Figure 1 with the same properties and excitation as in subsections 2.2 and 2.3. The critical damping ratio of the semi-active damper varies in the range 0–0.20. An AR model of adaptive order (subsection 3.2) based on $N = 250$ past samples with a sampling period $\Delta t = 0.01\ s$ is used to predict the earthquake excitation in a forward interval of 0.1 s at each instant.

First, the response to the Ardal record is studied. The results are compared to those obtained with the semi-active clipped-optimal algorithm of a previous work.[10] The semi-active control algorithm in this previous work is, in essence, the same as that presented in subsection 2.4 for the linear optimal case, except that it is clipped to the optimal solution of the linear homogeneous problem. That is, the target control force is determined using LQR. The results presented in Figure 11 confirm the efficacy of the proposed semi-active control algorithm. A substantial attenuation of the floor response spectra in the vicinity of the second eigen frequency (13.4 Hz) is achieved, which is superior to that obtained with the clipped-optimal control algorithm of Politopoulos and Pham,[10] whereas the peak amplitude at the first eigen frequency (0.5 Hz) is the same for both methods. This means that both design objectives (i.e., attenuation of the response of the isolated and non-isolated modes) are met to a higher degree when information on the excitation is taken into account as it is the case for the proposed algorithm.

The efficacy of the proposed semi-active control algorithm is further confirmed for other excitation signals. The additional four signals used in subsection 3.2, that is, two of the horizontal acceleration signals recorded during the main event of Tohoku earthquake on 11/03/2011 and two artificially generated signals compatible with Cadarache site in south France are also,

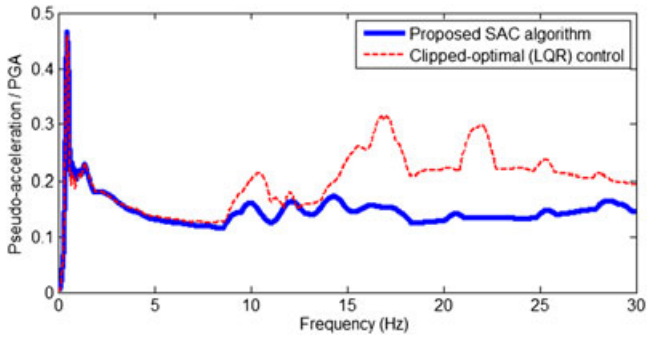

FIGURE 11 Normalized floor response spectrum at the base for Ardal signal for 2% damping. LQR = linear quadratic regulator; PGA = peak ground acceleration; SAC = semi-active control

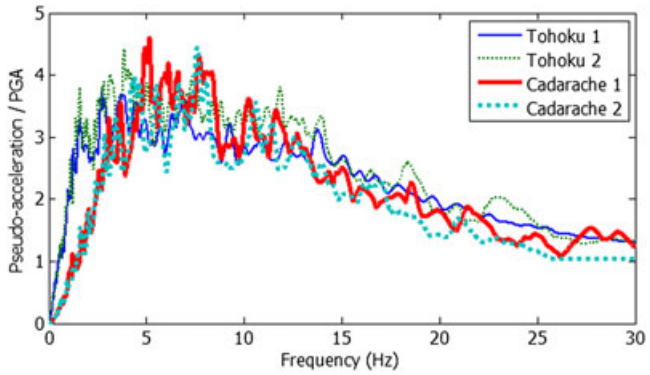

FIGURE 12 Normalized pseudoacceleration response spectra of Tohoku and Cadarache signals for 2% damping. PGA = peak ground acceleration

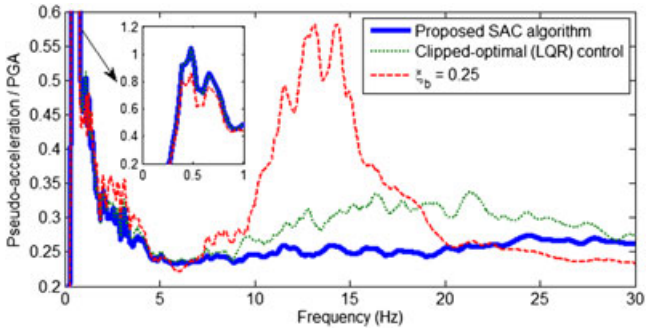

FIGURE 13 Mean normalized floor response spectrum at the base for Tohoku and Cadarache signals for 2% damping. LQR = linear quadratic regulator; PGA = peak ground acceleration; SAC = semi-active control

TABLE 1 Maximum base displacement per peak ground acceleration (m/g)

Control algorithm	Ardal	Cadarache 1	Cadarache 2	Tohoku 1	Tohoku 2
$\xi_b = 0.25$	0.0917	0.0854	0.0891	0.2050	0.2981
Clipped-optimal SAC	0.1068	0.1165	0.1063	0.2396	0.3531
Proposed SAC algorithm	0.1053	0.1178	0.1062	0.2376	0.3482

Note. SAC = semi-active control.

considered. Their normalized pseudoacceleration spectra for 2% damping are shown in Figure 12. Both pairs of signals have considerable energy in the vicinity of the second eigenfrequency of the structure, and the first one gives rise to considerable displacement of the isolator also. The mean normalized floor response spectra at the base for these signals are shown in Figure 13. Regarding the base displacement, Table 1 shows that, for the above signals, similar reduction is achieved by the two semi-active algorithms, considered in this section, and by enhanced passive damping.

5 | CONCLUSIONS

In this paper, a new semi-active control algorithm for mixed base isolated structures, combining both passive and semi-active devices, is investigated as a means to improve floor response spectra while limiting base displacements. It is hoped that a better response of the system may be achieved if the controller design accounts for the earthquake excitation and the control variable is directly the governing parameter of the semi-active device (e.g., damping constant in the case of a viscous semi-active damper). To this end, we propose a semi-active control algorithm based on an approximate iterative solution of a nonlinear inhomogeneous constrained optimal control problem. Because the inhomogeneous control techniques need upcoming excitation information, which is not available in real time control situations, an auto-regressive model is used to predict, at each control time step, the earthquake excitation over a short time interval ahead. To illustrate its efficacy, this algorithm has been applied to a simple two DOF base isolated structure equipped with a semi-active linear viscous damper. The analyses' results show that the proposed algorithm is capable to reduce the base displacement without significant amplification of the response of the non-isolated modes. Moreover, comparison with the well-known clipped-optimal control algorithm demonstrates the superiority of the new semi-active control algorithm.

Though the results presented in this paper are quite encouraging, it must be acknowledged that a lot of work should be still done before envisaging to apply this method to real structures. For instance, issues such as computation speed up, observers, measurement noise, time delay, and simultaneous control of several SAC devices should be studied for real-world applications. In addition, not all physical constraints of the SAC device have been included in the nonlinear optimal problem considered here. Actually, though NLQI accounts for the bounds of the damping coefficient, it does not account for the fact that the damper force cannot exceed a given value (i.e., saturation of the damper force). Another issue, which has to be investigated, is spillover. In fact, in practice, the design of the controller is based on a reduced model of the real structure whereas the control action is applied to the real structure, which has much more DOF. Hence, the response of the DOF not retained in the reduced model may have some undesirable effects and diminish the benefice expected from the proposed control algorithm.

ACKNOWLEDGEMENT

This work was partially funded by the "Institut Français de Radioprotection et de Sûreté Nucléaire" (IRSN).

REFERENCES

[1] J. M. Kelly, H. C. Tsai, *Earthq. Eng. Struct. Dyn* **1985**, *13*(6), 711.

[2] H. C. Tsai, J. M. Kelly, *Earthq. Eng. Struct. Dyn* **1988**, *16*(1), 29.

[3] I. Politopoulos, *Earthq. Eng. Struct. Dyn* **2008**, *37*(3), 447.

[4] C. Alhan, H. Gavin, *Eng. Struct.* **2004**, *26*(4), 485.

[5] S. Chimamphant, K. Kasai, *Earthq. Eng. Struct. Dyn.* **2016**, *45*, 5.

[6] C. Alhan, S. Oncu-Davas, *Eng. Struct.* **2016**, *116*, 83.

[7] I. Politopoulos, *Earthquake Eng. Struct. Dyn.* **2009**, *39*(3), 325.

[8] J. P. Wolf, P. Obernhuber, *Earthq. Eng. Struct. Dyn.* **1981**, *9*(1), 1.

[9] J. P. Wolf, P. Obernhuber, B. Weber, *Earthq. Eng. Struct. Dyn.* **1983**, *11*(4), 483.

[10] I. Politopoulos, H. K. Pham, *Bull. Earthq. Eng.* **2010**, *9*(4), 1115.

[11] S. J. Dyke, B. F. Spencer, M. K. Sain, J. D. Carlson, *Smart Mater. Struct.* **1998**, *7*(5), 693.

[12] M. D. Symans, M. C. Constantinu, *Earthq. Eng. Struct. Dyn.* **1997**, *26*(7), 759.

[13] S. Narasimhan. Control of smart base isolated buildings with new semi-active devices and novel H2/LQG, H∞ and time-frequency controllers. PhD Thesis. Rice University, Houston, TX, USA, 2004.

[14] S. Nagarajaiah, S. Narasimhan, *Earthq. Eng. Struct. Dyn.* **2007**, *36*(6), 729.

[15] G. Leitmann, *J. Intell. Mater. Syst. Struct.* **1994**, *5*, 841.

[16] N. H. McClamroch, H. P. Gavin, in *Proc. of the Amer. Ctrl. Conf.* **1995**; Seattle, Washington, 4173–77.

[17] R. Stengel, *Optimal control and estimation*, Dover Publications, New York **1986**.

[18] A. E. Bryson, Y. C. Ho, *Applied optimal control: Optimization, estimation, and control*, Taylor & Francis, New York, USA **1975**.

[19] T. T. Soong, *Active structural control: Theory and practice*, Longman Scientific & Technical, Essex, UK and John Wiley & Sons, New York, USA **1990**.

[20] T. T. Soong, M. C. Costantinou (Eds), *Passive and active structural vibration control in civil engineering*, Springer-Verlag, Wien-New York **1994**.

[21] A. Preumont, *Vibration control of active structures: An introduction*, Kluwer Acadelic Publishers, Dordrecht, Netherlands **2002**.

[22] J. N. Yang, A. Akbarpour, P. Ghaemmaghami, *J. Eng. Mech.* **1987**, *113*(9), 1369.

[23] J. Suhardjo, B. F. Spencer Jr., M. K. Sain, *J . struct. Safety* **1990**, *8*, 69.

[24] K. Yamada, T. Kobori, *Earthq. Eng. Struct. Dyn.* **1996**, *25*, 631.

[25] G. Mei, A. Kareem, J. C. Kantor, *Earthq. Eng. Struct. Dyn.* **1998**, *30*, 995.

[26] J. Rodellar, A. H. Barbat, J. M. Martin-Sanchez, *J. Eng. Mech.* **1987**, *113*(6), 797.

[27] P. Dorato, A. H. Levis, *IEEE Trans. Aut. Contr.* **1971**, *6*, 613.

[28] J. H. Jacobson, *IEEE Trans. Autom. Control* **1968**, *13*(6), 661.

[29] S. R. McReynolds, A. E. Bryson, *Paper presented at the Joint Automatic Control Conference*, Troy, New York, **1965**.

[30] J. H. Jacobson, *J. Optim. Theory Appl.* **1968**, *2*(6), 411.

[31] G. Zoutendijk, *Methods of feasible directions*, Elsevier Pub. Co., London **1961**.

[32] S. V. Vaseghi, *Advanced digital signal processing and noise reduction*, 4th ed., John Wiley & Sons Ltd, London, UK **2008**.

[33] S. J. Orfanidis, *Optimum signal processing: An introduction*, Second ed., Rutgers University, New Jersey, USA **2007**.

How to cite this article: Vu DC, Politopoulos I, Diop S. A new semi-active control based on nonlinear inhomogeneous optimal control for mixed base isolation. *Struct Control Health Monit*. 2018;25:e2032. https://doi.org/10.1002/stc.2032